Optoelectronics based on 2D TMDs and heterostructures

Nengjie Huo[1, §], Yujue Yang[1, §], and Jingbo Li[1, 2, †]

[1]School of Materials and Energy, Guangdong University of Technology, Guangzhou 510006, China
[2]Institute of Semiconductors, Chinese Academy of Sciences, Beijing 100083, China

Abstract: 2D materials including graphene and TMDs have proven interesting physical properties and promising optoelectronic applications. We reviewed the growth, characterization and optoelectronics based on 2D TMDs and their heterostructures, and demonstrated their unique and high quality of performances. For example, we observed the large mobility, fast response and high photo-responsivity in MoS_2, WS_2 and WSe_2 phototransistors, as well as the novel performances in vdW heterostructures such as the strong interlayer coupling, am-bipolar and rectifying behaviour, and the obvious photovoltaic effect. It is being possible that 2D family materials could play an increasingly important role in the future nano- and opto-electronics, more even than traditional semiconductors such as silicon.

Key words: 2D TMDs; heterostructures; optoelectronics; phototransistors
DOI: 10.1088/1674-4926/38/3/031002 **EEACC:** 2520

1. Introduction

Two-dimensional (2D) materials such as graphene and transition metal dichalcogenides (TMDs) are one of the most interesting research topics due to their unique physical properties and great potential in optoelectronic applications. For example, a graphene monolayer with carbon atoms tightly packed into a 2D honeycomb lattice has been proven to possess an exceptionally high carrier mobility exceeding 10^6 $cm^2/(V\cdot s)$ at 2 K and thus have great application potential in ultrafast photodetectors[1, 2]. However, the band gap of graphene is zero, which limits its applications as the semiconducting active channel in optoelectronics, such as the graphene transistors cannot be turned off due to the high carrier concentration. Graphene also has a very low absorption coefficient leading to very low photo-responsivity and external quantum efficiency (0.1%–0.2%)[3, 4]. Regarding this disadvantage, Konstantatos *et al*.[5] deposited lead sulphide (PbS) quantum dots on top of graphene as a sensitive layer. For these hybrid photodetectors, a huge photo-gain (G) was generated due to the high absorption of PbS QDs and high mobility of graphene as well as the efficient charge transfer at the interface.

In contrast to graphene, 2D TMDs with sizable bandgaps around 1–2 eV complement the disadvantages of graphene and attract a great deal of attention due to their interesting physical properties in nanoelectronics, sensing and photonics[6–11]. Early start of 2D TMDs is WSe_2 crystal which exhibits high mobility (500 $cm^2/(V\cdot s)$), ambipolar behaviour and 10^4 on/off ratios at 60 K[12]. Then mono or few layer MoS_2 emerged as an interesting material in field effect transistors with excellent on/off ratio (10^8) and room-temperature mobility of 200 $cm^2/(V\cdot s)$[13, 14]. Compared to graphene-based devices, MoS_2 based photodetectors can exhibit enhanced responsivity and selectivity with improved responsivity (0.57 A/W) and fast photoresponse (70–110 ms); monolayer MoS_2-based photodetectors have been demonstrated with a maximum photo-responsivity of 880 A/W[15]. The bulk TMDs (MoS_2, WS_2) will become direct bandgap semiconductors when thinned to the monolayer limit. This bandgap transition facilitates the stronger optical emission and absorption, enabling high photon-mater interaction and high efficiency photovoltaic properties. The excellent electrical and optical features including the high mobility and tremendous gate modulation of current as well as strong photoluminescence could offer their opportunity in optoelectronics and energy harvesting applications. Besides, the TMDs based photodetectors show a huge internal photo-gain effect along with the very low dark current by operating the devices in depletion mode, which could produce extremely high responsivity and high sensitivity. Through encapsulation, plasmonic technique and quantum dots (PbS) sensitizing, the performances of TMDs based phototransistors can be further much improved with enhanced mobility and an extended spectrum region into the near and short-infrared spectrum, which is important in the night version, remote sensing and communications. Besides, TMDs also demonstrate the advantages in the molecular sensing applications due to the high surface-to-volume ratio. For instance, single and few-layer MoS_2 sheets have been demonstrated to be sensitive detectors for NO, NO_2, NH_3 and trimethylamine gas. The detection mechanism is probably due to the n-doping or p-doping induced by the adsorbed gas molecular, changing the resistivity of the intrinsically n-doped MoS_2. Another interesting and important feature of atomically thin 2D materials is the large mechanical and bendable characteristics enabling the flexible and wearable sensors and detectors. Recently, other 2D TMDs such as $MoSe_2$, WS_2, WSe_2 etc. and the new 2D family materials such as black phosphorus have also shown great application potential in transistors, photodetectors and gas sensors.

Van der Waals heterostructures assembled by individual 2D layers are currently gaining particularly attention owing to their broad-range of optical bandgap and strong light-matter interactions[16, 17]. It is proved that TMDs based heterostructures

§ These authors contributed equally to this work.
† Corresponding author. Email: jbli@semi.ac.cn
Received 27 September 2016, revised manuscript received 13 January 2017

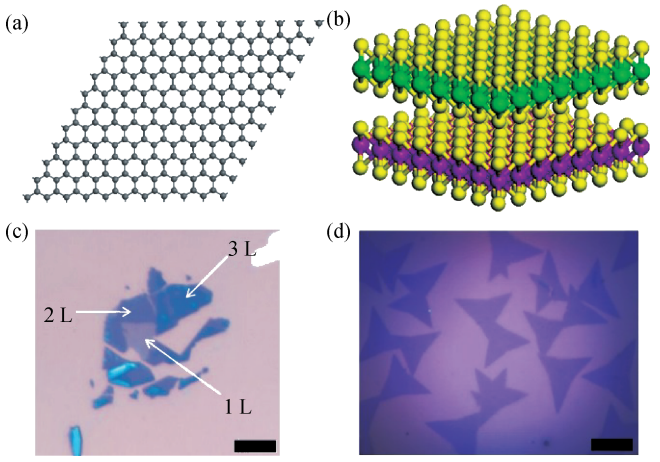

Fig. 1. (Color online) (a, b) Schematic diagram of graphene and TMDs (MoS_2 or WS_2), respectively. (c, d) Optical microscopy images of exfoliated WSe_2 and CVD grown MoS_2, respectively. The scale bar is 10 μm.

usually possess type-II band alignment, which can facilitate the efficient electron-hole separation[18–20]. For example, MoS_2 /WS_2 heterostructure can exhibit novel and enhanced optoelectronic performances including the bipolar doping and photovoltaic properties [21]. More recently, growing interest has been focused on the p–n van der Waals (vdW) heterostructures since the p–n diode is one of the most fundamental building blocks of modern electronics and optoelectronics. In our recent research work, we found that the p–n WSe_2/MoS_2 heterostructures could exhibit strong interlayer coupling and distinct current rectification behaviour [22]. Interesting tunable polarity behaviour has also been observed in the WS_2/WSe_2 p–n junctions [23]. Actually there exist large numbers of 2D TMDs that can be exfoliated and CVD grown easily and assembled to design various heterostructures, which can provide an important platform for developing next-generation electronics and optoelectronics. In this work, we will introduce the development of 2D materials including the growth, physical properties and their optoelectronic applications in transistors, photodetectors and solar cells.

2. Growth and methods

Graphene is the monolayer counterpart of graphite which possesses a hexagonal honeycomb structure (Fig. 1(a)). 2D TMDs such as MoS_2 and WS_2 possess similar crystalline structures in which each single plane of MS_2 (M: Mo or W) comprises a trilayer composed of a molybdenum or a tungsten layer sandwiched between two sulphur layers in a trigonal prismatic coordination (Fig. 1(b)). Compared to the traditional materials, the new 2D materials exhibit very unique and excellent physical and chemical properties. Before discussing their optoelectronic properties, we firstly introduce the growth and some methods involved in this paper.

Geim *et al.* developed a very facile tap exfoliation method to prepare the monolayer graphene in 2004 and thus won the Nobel fellowship in 2012 because of his contribution to graphene. Afterward, this simple method has also been proved useful in fabricating other 2D materials such as MoS_2 thus extending the studies based on these monolayer materials. For any scientific research, the high quality of materials is most important as a basic fundamental. The exfoliated MoS_2 exhibits high optoelectronic properties such as the high photoluminescence and mobility, but the size of the samples using the exfoliated method is very small, which limits their wide applications in an actual product. Thus the CVD method for large area and high quality of MoS_2 has been investigated extensively.

2.1. Mechanical exfoliation

2D crystals such as MoS_2, and WS_2 slice were purchased from Lamellae Co. and pasted on magnetic adhesive tape. Folding the sticky side of the tape in half then tearing the tape very slowly, thus the 2D slices are divided into two. This operation is repeated many times until very thin nanoflakes are exfoliated on the tape. The nanoflakes were exfoliated onto SiO_2/Si substrate by pressing the tape gently and then removing it slowly. After the exfoliation, the substrate was placed into hot acetone to remove the residual glue. Thus the 2D materials with different layers can be prepared on the substrate (Fig. 1(c)). The materials using this method usually have large mobility and high photo-response, but the disadvantage is the very small size which limits their large scale applications in optoelectronics.

2.2. CVD growth

2D materials (MoS_2) can be grown on different substrates, such as the SiO_2 and sapphire. Before growth, the substrate should be cleaned in acetone, isopropanol and DI water, followed by 5 min of O_2 plasma. They were then loaded into a 1-inch CVD furnace and placed face-down above a crucible containing 10 mg of MoO_3 (99.8% Sigma Aldrich) with another crucible containing 100 mg of sulphur (99.5% Sigma Aldrich) located upstream. The CVD growth is performed at atmospheric pressure while flowing ultrahigh-purity nitrogen at 700 ℃ for 10 min. Then the furnace is opened, the N_2 flow is increased and it is cooled down to room temperature. Fig. 1(d) shows the triangle MoS_2 single crystal using the CVD method. This method can produce large scale 2D materials and facilitate actual applications in the future; however, some problems with the CVD method still remain such as there are lots of defects and low mobility.

2.3. Transfer methods for heterostructures

In the case of MoS_2–WS_2 heterostructures: The MoS_2–WS_2 heterostructures were fabricated with the dry transfer method. Firstly, the multilayer MoS_2 and WS_2 nanoflakes were exfoliated onto two pieces of SiO_2/Si (300 nm SiO_2) substrates respectively from the MoS_2 and WS_2 crystals (2D semiconductors.com) with the micromechanical cleavage approach. Secondly, the polymethyl methacrylate (PMMA) liquid was spin-coated on the substrate with WS_2 nanoflakes with a rotating speed of 4000 r/s. After annealing with 150 °C for 30 min, the substrate with PMMA film was soaked into the 2 M NaOH solution. Then, the PMMA film with WS_2 nanoflakes was floated and transferred onto another substrate to overlap with the MoS_2 nanoflakes. Finally, the PMMA was dissolved by acetone and the stacked MoS_2–WS_2 heterostructures were achieved.

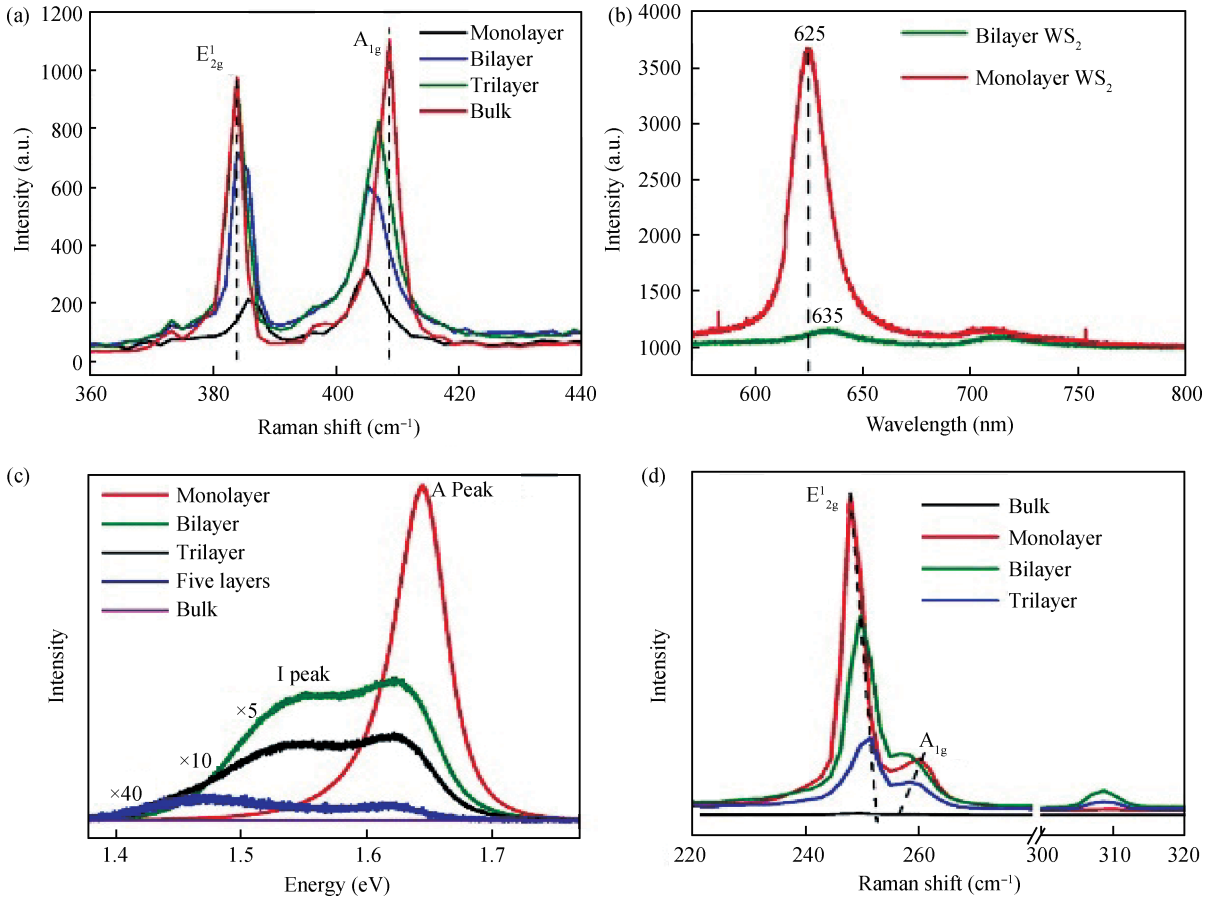

Fig. 2. (Color online) (a) Raman spectra of MoS_2 layers with different layers. (b) PL spectrum of monolayer and bilayer WS_2. (c, d) PL and Raman spectrum of WSe_2 with different layers.

2.4. Nano-devices fabrication

The general nano-device fabrication technique is photolithography such as the EBL and laser writer, but the fabrication cost is very high. In this work, we used the home-made and low-cost "gold-wire mask moving" technique. Firstly, MoS_2 flakes was exfoliated from the MoS_2 crystals onto 300 nm SiO_2/Si substrates using the mechanical exfoliation technique, and with vacuum annealing at 350 °C for 2 h to remove the residual glue. Secondly, a micron gold-wire serving as a mask was fixed tightly on the top surface of WS_2 nanoflakes, and then a pair of Au electrodes was deposited onto the substrate by thermal evaporation. To avoid the scattering of metallic atoms onto the side-face of SiO_2/Si substrates, the sides of the substrate were covered with tin foil. Finally, by slightly removing the Au wire mask and tin foil, the Au electrodes were fabricated and a micron size gap was produced between the two electrodes.

3. Optical properties (PL and Raman)

Generally, the band structure and phonon frequency of MS_2 layers are very sensitive to the thickness, i.e. indirect bulk MS_2 can turn into direct bandgap materials when thinned to monolayer, the Raman active mode A_{1g} (out-of-plane displacement of S atoms) stiffens, and the E^1_{2g} (in-plane displacement of M and S atoms) softens with increasing number of layers, as shown in Fig. 2(a) for MoS_2. Fig. 2(b) shows the PL spectrum of WS_2. The PL intensity decreased with the increased layers. For 2D WSe_2 layers, the crystalline structure is similar to MoS_2 and WS_2. The indirect-to-direct band gap crossover with decreasing layers to monolayer can also happen from the photoluminescence (PL) spectra (Fig. 2(c)). The monolayer WSe_2 exhibits a strong direct transition emission "A" peak at the energy of 1.65 eV. For the bilayer WSe_2, the "A" peak becomes one order of magnitude weaker and red-shifts by about 20 meV, accompanied by the emerging indirect transition emission "I" peak at the energy of 1.55 eV. The "I" peak further shifts toward lower energy and outweighs the "A" peak at five layers. No PL signal is observed in bulk WSe_2[22].

In contrast, the WSe_2 layers exhibit abnormal Raman modes where the Raman intensity is very sensitive to the thickness and decreases sharply with increasing number of layers (Fig. 2(d)). The Raman intensity of bulk WSe_2 is negligible, which is starkly different with MoS_2. The reason for the unique Raman intensity of WSe_2 can be attributed to the strong interaction with the SiO_2 capping[24]. For the phonon frequency, unlike the obvious separated E^1_{2g} and A_{1g} modes in MoS_2 and WS_2, two adjacent modes at around 250 nm are assigned to E^1_{2g} and A_{1g} modes, respectively[25, 26]. Moreover, the E^1_{2g} mode stiffens and A_{1g} softens with increasing thickness of WSe_2 layers leading to the largest frequency differences in monolayer WSe_2. The monolayer WSe_2 is most affected by the strain effect resulting in most severe splitting[22]. Overall, the sensitiv-

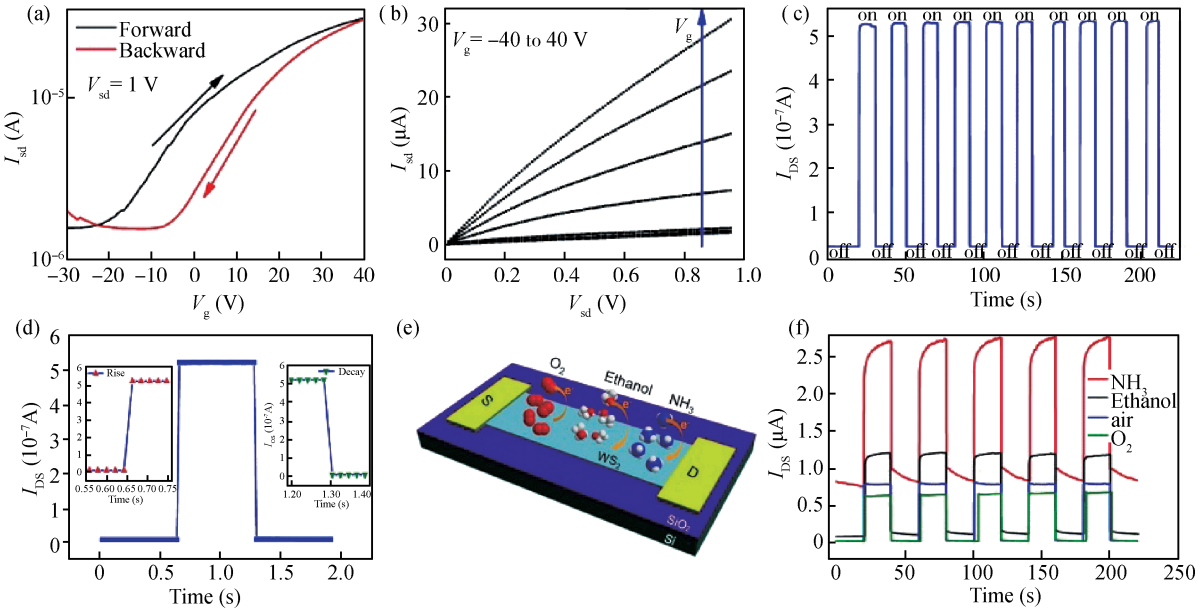

Fig. 3. (Color online) (a) Transfer curves of WS_2 based transistors. (b) Output curves of WS_2. (c, d) Dynamic response of WS_2 phototransistors. (e) Schematic diagram of the device with different gas molecules. (f) Photoresponse under different gas atmosphere[27].

ity change of phono frequency and PL intensity with various thicknesses in 2D family materials could be a quick and convenient identification of different layers.

4. Optoelectronic applications: FETs, photodetectors and solar cells

2D materials have been demonstrated to have great application potential in various optoelectronics such as transistors, photodetectors and solar cells. In the following we will introduce the excellent properties of the 2D TMDs in these optoelectronics.

The mobility, photoresponsivity R and external quantum efficiency EQE are critical figures of merit for transistors and photodetectors. The large values of mobility, R and EQE correspond to high quality materials and high light sensitivity.

The mobility (μ) can be obtained from the equation $\mu = \frac{\partial I_{DS}}{\partial V_G}\frac{L}{WC_iV_{DS}}$, where L is the channel length, W is the channel width, and C_i is the gate capacitance between the channel and the silicon back gate per unit area, which can be given by equation $C_i = \varepsilon_0\varepsilon_r/d$, ε_0 is the vacuum dielectric constant, and ε_r (3.9) and d(300 nm) are dielectric constant and thickness of SiO_2, respectively.

R and EQE can be expressed as $R_\lambda = I_{ph}/PS$, EQE $= hcR_\lambda/e\lambda$, where I_{ph} is the photo-excited current; P is the light power intensity; S is the effective illumination area; h is Planck's constant; c is the velocity of light; e is the electron charge; and is the excitation wavelength.

4.1. WS_2 based phototransistors

The multilayer WS_2 phototransistors were fabricated using the gold wire mask method. From the transfer and output characteristic (Figs. 3(a) and 3(b)), we get that the drain current increases largely with increased gate voltage indicating the n-type behaviour. The electron mobility can be calculated to be 12 $cm^2/(V{\cdot}s)$. With light irradiation on/off, the device can also work between low and high impedance states fast and reversibly with an on/off ratio of 25, allowing the device to act as a high quality photosensitive switch. The device also exhibits very fast dynamic response for both rise and decay processes (Figs. 3(c) and 3(d)): the response time is shorter than 20 ms (detection limit of our measurement setup).

The photosensitive properties of the multilayer WS_2 nanoflakes under the various gas environments were also investigated. From the time dependence of the photocurrent at various gas atmospheres during the light switching on/off (Fig. 3(f)), the WS_2 phototransistors can respond to the given gas molecules sensitively which play a different role in the conductivity and photosensitive properties. The drain current of the device is decreased at O_2, but increased at ethanol and NH_3. This is from the charge transfer between the WS_2 nanoflakes and the adsorbed gas molecules as shown in Fig. 3(e). Once the vapour molecules come into contact with the surface of WS_2, the gas molecule would be adsorbed, subsequently changing the charge carrier distribution in WS_2 nanoflakes. O_2 molecules can act as electron acceptors to accept electrons from WS_2, leading to a reduction in overall conductivity. In contrast, ethanol and NH_3 molecules, serving as electron donors, can donate electrons to the WS_2 nanoflakes, which enhance the total conducting electrons density, resulting in the increased current. It is noted that the R and EQE of the multilayer WS_2 nanoflakes photodetectors at air are 5.7 A/W and 1118%, respectively, which further improved to 884 A/W and 1.7×10^5% under the NH_3 atmospheres[27], demonstrating that the 2D multilayer WS_2 nanoflakes can be effectively used in highly sensitive photodetectors and fast photoelectric switches.

4.2. MoS_2 and WSe_2 based phototransistors

Fig. 4(a) shows the transfer curves of the few-layers MoS_2 which performs very well n-type behavior with a large on/off

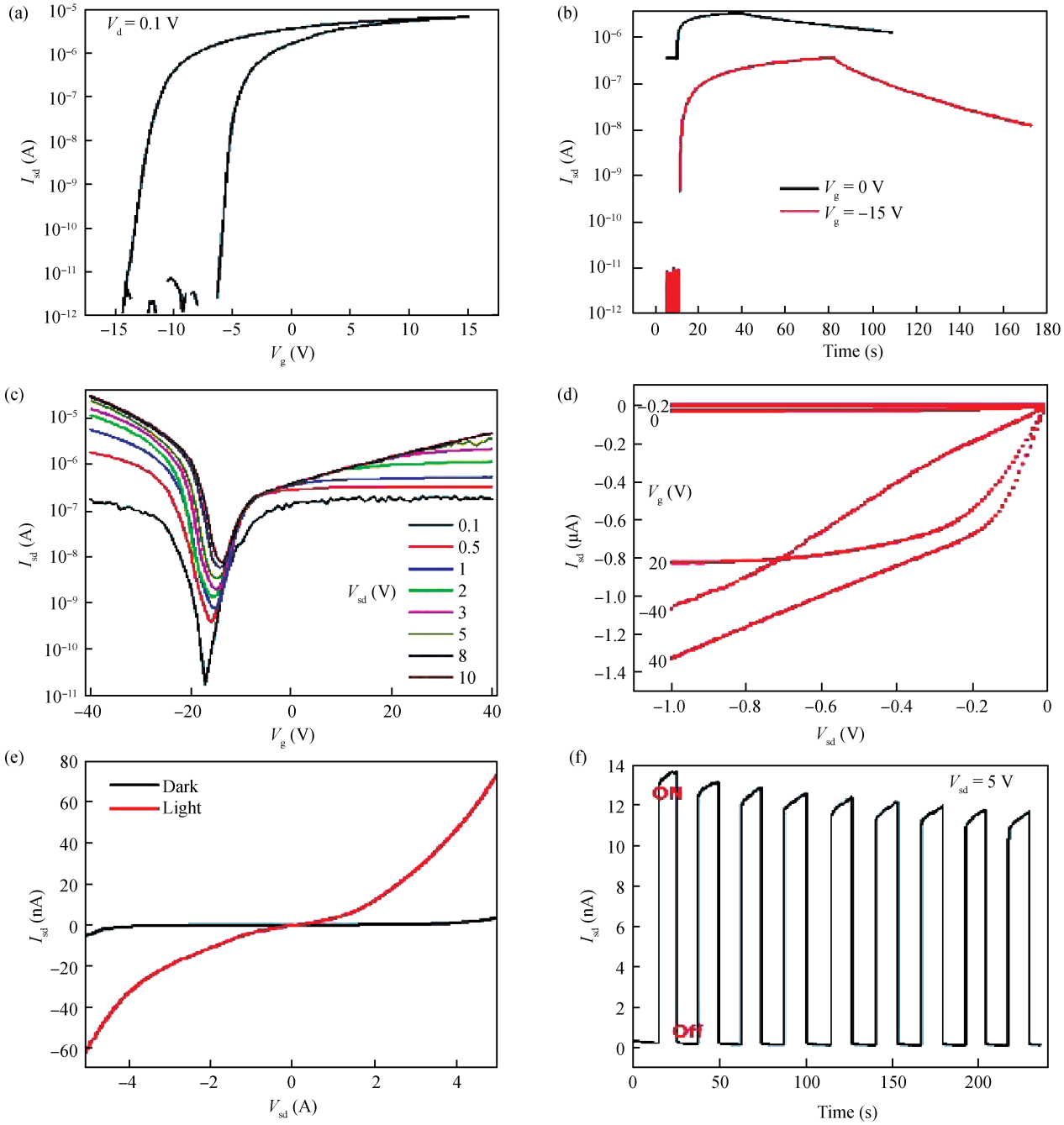

Fig. 4. (Color online) (a) Transfer and (b) output characteristics of pure atomically thin MoS_2 layers, the I_{sd} can increase with increasing gate voltage and the on/off ratio can reach higher than 10^6, indicating the well n-type behaviour of MoS_2 layers. (c) Transfer and (d) output characteristics of pure atomically thin WSe_2 layers, indicating the well p-type behavior of WSe_2 layers with on/off ratio of about 10^4. (e) I–V curves of WSe_2 transistors under dark and light. (f) Dynamic response of WSe_2 devices.

ratio of 10^6 and large electron mobility; from the output characteristics, it is the Ohmic contact between Ti/Au electrodes and MoS_2 channel. The high performance of MoS_2 transistors indicates its great application potential in future nanoelectronics and integrated circuits. But the photo-response is very slow due to the large amounts of defects such as the H_2O and O_2 absorbed on the surface of MoS_2. Fig. 4(b) shows the time dependences of drain current under the different gate voltage. Once light illuminated the devices, the current increases relatively fast but decreases very slowly once the light is turned off, even the current cannot recover to the initial value. It is also found that under the negative gate voltage (−15 V) the dark current is very small (pA) resulting in the low noise and high sensitivity. The photocurrent is over 200 nA and photo-responsivity is calculated to be 1057 A/W, which is much higher than that under zero gate (63 A/W). As the slow response limits their application in photodetectors, different methods have been tried in attempts to improve the performances. For example, after the encapsulation with ALD Al_2O_3 the performances of MoS_2 phototransistors are much improved with a fast response of only

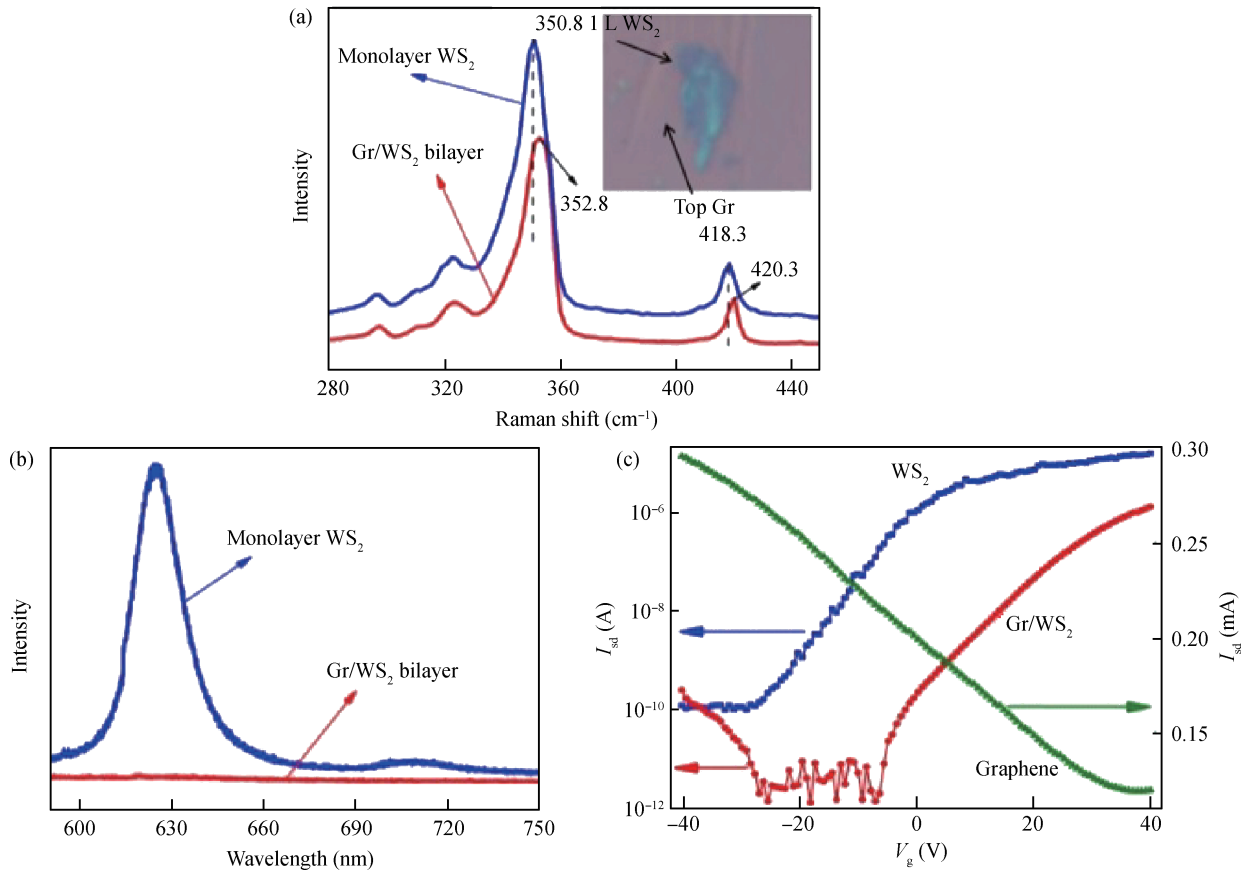

Fig. 5. (Color online) (a) Raman and (b) PL spectra of monolayer WS_2 and the bilayer graphene/WS_2 heterostructure. The inset of (a) is an optical image of graphene/WS_2 bilayer. (c) Transfer curves of graphene, WS_2 and Gr/WS_2 devices[29].

10 ms[28].

In contrast to the n-type of WS_2 and MoS_2 as discussed above, the WSe_2 can exhibit different behaviors depending on the contact metal. Based on the previous literature, the Ag metal with low work function can lead to the n-type behavior of WSe_2 but the metal with high work function such as Pd or Pt can result in the p-type behavior because the high work function metal can facilitate the holes transport in the WSe_2 channel. Here we used Au as the source and drain electrodes and found the ambipolar behavior as shown in the Fig. 4(c). The on/off ratio ranged from 10^3 to 10^4 with varying bias for both electrons and holes. The output curves (Fig. 4(d)) also demonstrated the typical ambipolar behavior. From both I–V and I–t curves (Figs. 4(e) and 4(f)), the drain current is much improved under light illumination and the response is very fast with a raise and delay time of only 20 ms indicating the sensitive photo-detections.

5. Heterostructures based on the 2D materials

5.1. WS_2–graphene heterostructures

The van der Waals heterostructures are assembled by individual 2D layers using the transfer method. Due to the broad-range of optical bandgap and strong light-matter interactions, they exhibit unique and excellent properties and thus are gaining particular attention. Now we will introduce some interesting optoelectronic properties in different heterostructures. Figs. 5(a) and 5(b) show the Raman spectrum of bilayer graphene–WS_2 heterostructures, which exhibited distinctive Raman and PL characteristics compared with each constituent layer. First-principles calculations showed that graphene bound to the WS_2 monolayer with an interlayer spacing of about 3.9 Å indicated a strong interaction between graphene and WS_2 (MoS_2) monolayers. The Raman modes A_{1g} and E^1_{2g} significantly stiffen by 2 cm^{-1} in this bilayer heterostructure, implying the strong interlayer coupling between graphene and WS_2. We found that both A_{1g} and E^1_{2g} modes of WS_2 stiffen by coupling with graphene. Considering the strong interlayer coupling between graphene and WS_2, two possible physical models were proposed to explain the phonon stiffening in Gr–WS_2 heterostructures[29]. One is the electron–phonon interaction model, where lower electron concentration leads to weaker electron–phonon coupling, and thus induced stiffening in the Raman modes A_{1g}. The other model is the interlayer interaction. The strong interlayer coupling between graphene and WS_2 can surpass the Coulomb interactions and strengthen both in-plane and out-of-plane effective restoring forces acting on the atoms, hence resulting in the higher frequencies of A_{1g} and E^1_{2g} modes.

Fig. 5(c) shows the typical transfer characteristics of WS_2, graphene and Gr–WS_2 heterostructure separately. The ultrathin WS_2 layers and monolayer graphene exhibit n-type and p-type behavior respectively. However, the Gr–WS_2 heterostructures exhibited obvious ambipolar properties with a high n-type on/off ratio of almost 10^6 and a p-type on/off ratio of about 10^2,

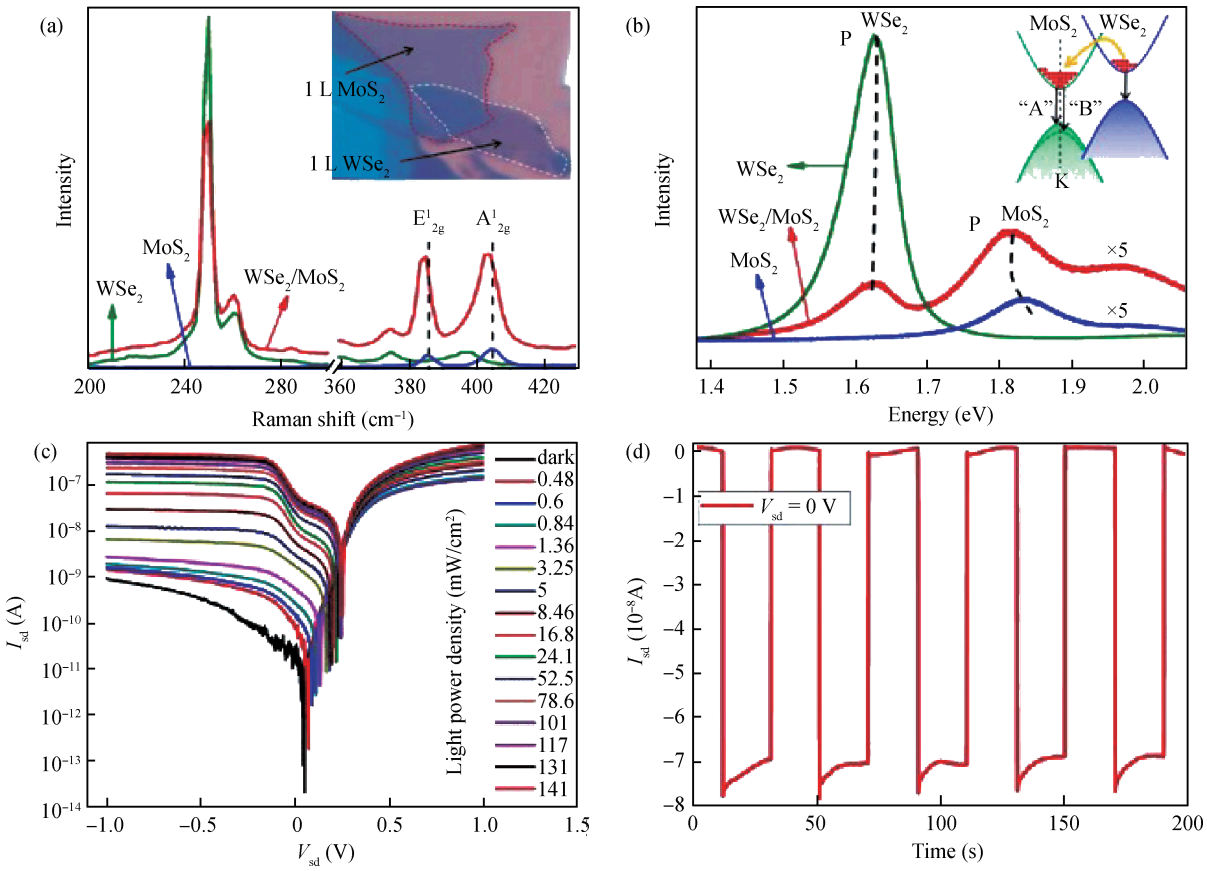

Fig. 6. (Color online) (a, b) Raman and PL spectrum of MoS_2/WSe_2 heterostructures, respectively. (c) I–V curves of MoS_2/WS_2 heterojunctions under light illumination with different light power. (d) Dynamic response under zero bias[21, 22].

which could be derived from n-type WS_2 and p-type graphene. Gate-induced electrons in WS_2 were dominated under positive V_g, thus forming an n-type conducting channel. But, the electrons in WS_2 were exhausted under negative V_g and the holes from the p-type graphene can modulatingly dope the WS_2 at the interface, resulting in the p-type behavior[29].

5.2. MoS_2–WSe_2 (WS_2) heterostructures

The monolayer MoS_2 and monolayer WSe_2 are vertically stacked forming the bilayer heterostructures (inset of Fig. 6(a)). In the WSe_2 /MoS_2 bilayers, the typical Raman modes A_{1g} and E^1_{2g} of both MoS_2 and WSe_2 monolayers appear at the same frequencies as in their isolated monolayers (Fig. 6(a)), indicating that the interlayer coupling is very weak between the constituent layers. The PL signal in the heterostructures changes greatly: emission from WSe_2 sharply drops and emission from MoS_2 slightly increases (Fig. 6(b)). This is probably from the inefficient charge transfer due to the very weak interlayer coupling[22].

We now turn into the MoS_2/WS_2 heterojunctions. Similar Raman and PL spectrum of the heterostructures were observed in MoS_2/WSe_2 heterostructures. The interesting point is that we made the vertical and planar transistors based on the multilayer MoS_2–WS_2 heterostructures and found novel and excellent field-effect and photosensitivity with new functionalities and superior electrical and optoelectronic properties that far exceed the one for their constituents. The vertical device exhibits a rectifying property with forward to reverse bias current ratios of 10^3 and a bipolar behaviour, which has an n-type behavior with an ON/OFF ratio of more than 10^4 under positive V_{sd} and a p-type behavior with an ON/OFF ratio of 10 times under negative V_{sd}. The observed behaviour can be attributed to the type-II band alignment between MoS_2 and WS_2 and the band slope induced by the gate voltage[21]. Fig. 6(c) shows I–V curves under dark and upon light illumination with different light power density, depicting the formation of short-circuit current I_{sc} and open circuit voltage V_{oc} upon light illumination, which increases with the light power, indicating an excellent photovoltaic property. The maximum V_{oc} can reach 0.25 V. Another important phenomenon is that the vertical transistors can also perform as a self-driven photodetector without applying source-drain bias (Fig. 6(d)), and the photocurrent can change sensitively and rapidly with light switching on/off[22].

5.3. WS_2–WSe_2 PN heterojunctions

Moreover we also investigated the p-WSe_2/n-WS_2 heterojunctions and demonstrate their unusual electrical transport and photo-responsive properties. Obvious current rectification and symmetrical ambipolar characteristics as well as large current hysteresis are observed in this artificial heterojunction. Interestingly, the polarity behaviours of the heterostructures system can be modulated by source drain voltage V_{sd} and gate voltage V_g ranging from n- or p-type to ambipolar or "anti-bipolar" behaviour. A unique transport model is proposed to explain this

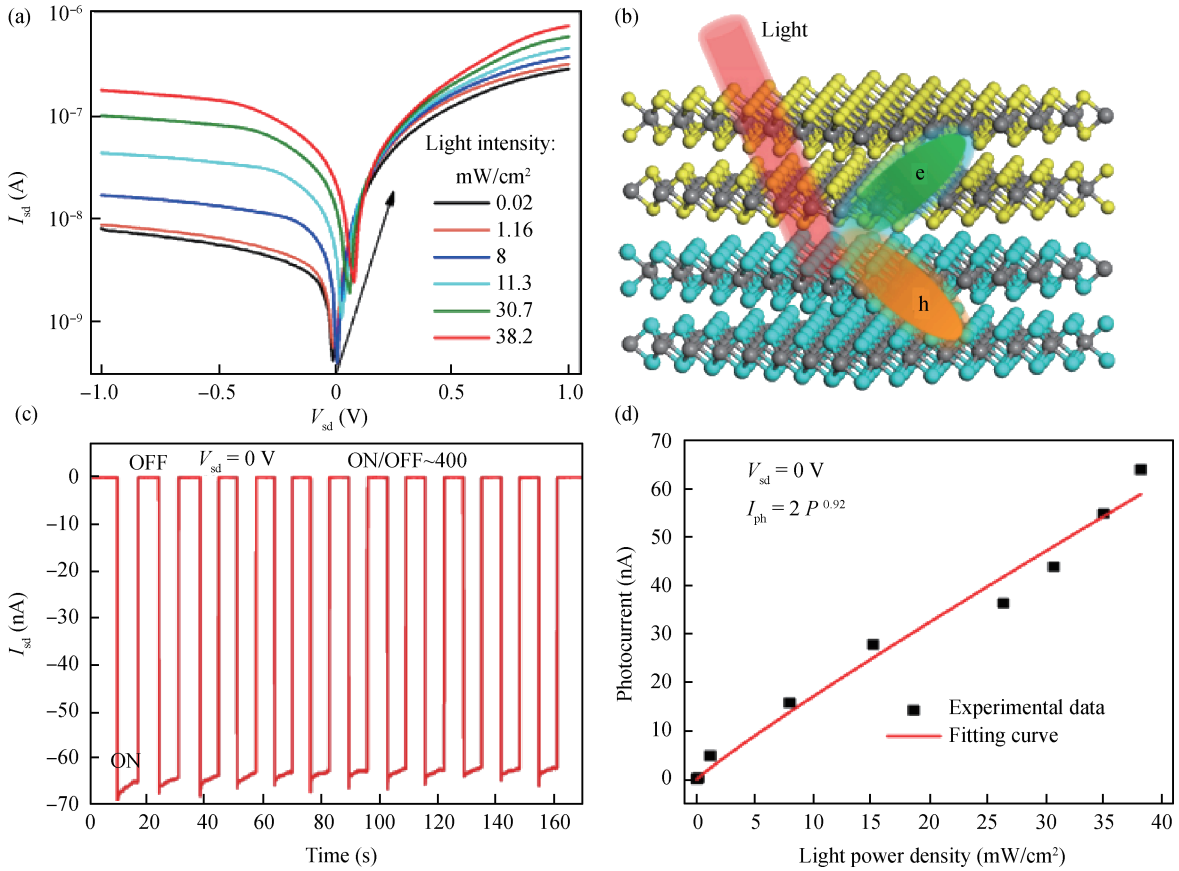

Fig. 7. (Color online) (a) I–V curves of WS_2–WSe_2 PN heterojunctions under light with different light power density. (b) Schematic diagram of photo-generated electron–hole separation in this junction. (c) Time dependences of I_{sd} during the incident light switched on/off. (d) Photocurrent as function of light power density with V_{sd} of 0 V[23].

phenomenon in which the conducting channels of junctions, p-WSe_2 and n-WS_2 will successively work on electrical transport with gradually improving V_{sd}[23].

Like the MoS_2/WS_2 heterostructures, the p–n junctions also exhibit excellent photovoltaic, self-driven and enhanced photo-switching properties. Fig. 7(a) shows I_{sd}–V characteristics of the heterojunctions devices under light illumination (633 nm) with different incident light power densities. With the increasing light power, the open-circuit voltage V_{oc} and short-circuit current I_{sc} are forming and increasing, indicating the excellent photovoltaic properties. Due to the energy gradient from type-II band alignment and the built-in potential between WSe_2 and WS_2, the photo-excited electron-hole pairs can be efficiently separated (Fig. 7(b)). Under light illumination, the photo-excited electrons in WSe_2 and holes in WS_2 can easily drift into the other layer, thus resulting in the significant photocurrent and photovoltaic effect. From the dynamic response of photocurrent with zero bias (Fig. 7(c)), the photocurrent can be produced and annihilated quickly and sensitively with the light switching on/off. The photo-switching on/off ratio can reach higher than 400 times and the response time is less than 20 ms revealing the high efficient electron–hole separation and high quality of self-driven photo-switching[23].

6. Conclusion

In summary, the growth, characterization and nano-devices performances of 2D materials (graphene and TMDs) and their heterostructures were systemically introduced. The 2D TMDs were prepared by CVD and the exfoliation method, which can exhibit excellent performances of phototransistors with high mobility and fast response. The heterostructures were fabricated by stacking different 2D layers on top of each other, which also performs unique physical and device properties such as the enhanced performances, strong interlayer coupling as well as high photovoltaic effect. All results demonstrate their huge application potential in future electronic and optoelectronic fields.

References

[1] Elias D C, Gorbachev R V, Mayorov A S, et al. Dirac cones reshaped by interaction effects in suspended graphene. Nat Phys, 2011, 7: 701

[2] Geim A K, Novoselov K S. The rise of graphene. Nat Mater, 2007, 6: 183

[3] Mueller T, Xia F, Avouris P. Graphene photodetectors for high-speed optical communications. Nat Photonics, 2010, 4: 297

[4] Nair R R, Blake P, Grigorenko A N, et al. Fine structure constant defines visual transparency of graphene. Science, 2008, 320: 1308

[5] Konstantatos G, Badioli M, Gaudreau L, et al. Hybrid graphene-quantum dot phototransistors with ultrahigh gain. Nat Nanotechnol, 2012, 7: 363

[6] Tsai D S, Liu K, Lien D H, et al. Few-layer MoS_2 with high

broadband photogain and fast optical switching for use in harsh environments. ACS Nano, 2013, 7: 3905
[7] Tongay S, Zhou J, Ataca C, et al. Broad-range modulation of light emission in two-dimensional semiconductors by molecular physisorption gating. Nano Lett, 2013, 13: 2831
[8] Hu P A, Wang L, Yoon M, et al. Highly responsive ultrathin GaS nanosheet photodetectors on rigid and flexible substrates. Nano Lett, 2013, 13: 1649
[9] Hu P A, Wen Z, Wang L, et al. Synthesis of few-layer GaSe nanosheets for high performance photodetectors. ACS Nano, 2013, 6: 5988
[10] Liu W, Kang J, Sarkar D, et al. Role of metal contacts in designing high-performance monolayer n-type WSe_2 field effect transistors. Nano Lett, 2013, 13: 1983
[11] Mak K, He K, Shan J, et al. Control of valley polarization in monolayer MoS_2 by optical helicity. Nat Nanotechnol, 2012, 7: 494
[12] Podzorov V, Gershenson M E, Kloc C, et al. High-mobility field-effect transistors based on transition metal dichalcogenides. Appl Phys Lett, 2004, 84: 3301
[13] Ayari A, Cobas E, Ogundadegbe O, et al. Realization and electrical characterization of ultrathin crystals of layered transition-metal dichalcogenides. J Appl Phys, 2007, 101: 014507
[14] Radisavljevic B, Radenovic A, Brivio J, et al. Single-layer MoS_2 transistors. Nat Nanotechnol, 2011, 6: 147
[15] Lopez-Sanchez O, Lembke D, Kayci M, et al. Ultrasensitive photodetectors based on monolayer MoS_2. Nat Nanotechnol, 2013, 8: 497
[16] Britnell L, Gorbachev R V, Jalil R, et al. Field-effect tunnelling transistor based on vertical graphene heterostructures. Science, 2012, 335: 947
[17] Yu W J, Li Z, Zhou H L, et al. Vertically stacked multi-heterostructures of layered materials for logic transistors and complementary inverters. Nat Mater, 2013, 12: 246
[18] Gong C, Zhang H, Wang W, et al. Band alignment of two-dimensional transition metal dichalcogenides: application in tunnel field effect transistors. Appl Phys Lett, 2013, 103: 053513
[19] Kang J, Tongay S, Zhou J, et al. Band offsets and heterostructures of two-dimensional semiconductors. Appl Phys Lett, 2013, 102: 012111
[20] Komsa H, Krasheninnikov A. Electronic structures and optical properties of realistic transition metal dichalcogenide heterostructures from first principles. Phys Rev B, 2013, 88: 085318
[21] Huo N J, Kang J, Wei Z M, et al. Novel and enhanced optoelectronic performances of multilayer MoS_2–WS_2 heterostructure transistors. Adv Funct Mater, 2014, 24: 7025
[22] Hao N J, Tangay S, Guo W L, et al. Novel optical and electrical transport properties in atomically thin WSe_2/MoS_2 p–n heterostructures. Adv Electron Mater, 2015, 1: 1400066
[23] Huo N J, Yang J H, Huang L, et al. Tunable polarity behavior and self-driven photoswitching in p-WSe_2/n-WS_2 heterojunctions. Small, 2015, 11: 5430
[24] Wang Y, Ni Z H, Shen Z X. Interference enhancement of Raman signal of graphene. Appl Phys Lett, 2008, 92: 043121
[25] Zhao Y, Luo X, Li H, et al. Interlayer breathing and shear modes in few-trilayer MoS_2 and WSe_2. Nano Lett, 2013, 13: 1007
[26] Li H, Lu G, Wang Y, et al. Mechanical exfoliation and characterization of single- and few-layer nanosheets of WSe_2, TaS_2, and $TaSe_2$. Small, 2013, 9: 1974
[27] Huo N J, Yang S X, Wei Z M, et al. Photoresponsive and gas sensing field-effect transistors based on multilayer WS_2 nanoflakes. Sci Rep, 2014, 4: 5209
[28] Kufer D, Nikitskiy I, Lasanta T, et al. Hybrid 2D–0D MoS_2–PbS quantum dot photodetector. Adv Mater, 2015, 27: 176
[29] Huo N J, Wei Z M, Meng X Q, et al. Interlayer coupling and optoelectronic properties of ultrathin two-dimensional heterostructures based on graphene, MoS_2 and WS_2. J Mater Chem C, 2015, 3: 5467